ISSN 1392 - 1207. MECHANIKA. 2013 Volume 19(5): 567-574

Considerations upon a new tripod joint solution

S. Alaci*, F. C. Ciornei, C. Filote*****
**"Stefan cel Mare" University, Suceava, Univesitatii no.13, 720229 Suceava, Romania, E-mail: alaci@fim.usv.ro*
***"Stefan cel Mare" University, Suceava, Univesitatii no.13, 720229 Suceava, Romania, E-mail: florina@fim.usv.ro*
****"Stefan cel Mare" University, Suceava, Univesitatii no.13, 720229 Suceava, Romania, E-mail: filote@eed.usv.ro*

crossref http://dx.doi.org/10.5755/j01.mech.19.5.5539

1. Introduction

Engineering solutions are often required concerning the transmission of rotary motion with constant transmission ratio between shafts with random axis position. When the relative position of the axes is constant in time the most convenient solution consists in using gear mechanisms. For the case of intersecting axes, the solution given in 1926 by Rzeppa is well-known [1] but the interest of this transmission is considerable and new technological solutions are permanently created [2]. The problem is more complex when the relative position of the axes is variable in time and one of the solutions is known as constant velocity joints (CV joints) or homokinetic joints. For the general case, the solution is given by the homokinetic mechanisms, as exposed by Seherr-Thoss et al. [3] and amongst these mechanisms, the tripod joints are met. Modern studies upon mechanisms apply both analytical methods, for the cases of rigid elements models, and numerical for deformable elements, validated by experimental work. In the present paper, analytical solutions are deduced for the general tripod transmission that applied for a specific chosen case becomes a tripod CV joint. Moreover, there is presented a structurally optimized tripod joint together with a proposed solution for reducing the contact wear.

2. Tripod joint structure

Motion transmission between the two elements is obtained via three joints. Depending on the structural solution and technical construction of the joints, several solutions for these couplings occur. The most widespread one, analyzed amid others, by Watanabe et al. [4] Mariot and K'nevez [5] Urbinati and Pennestri [6] Wang et al. [7] presents three point-line joints in its structure. The point-line joint can be materialized by a combination of low pairs and higher pairs. The structural scheme of a transmission via a tripod joint is presented in Fig. 1, where P is the plane joint, R_1, R_2 are the revolute joints and C_1, C_2, C_3 are the point-line joints. The technical solution consists of three spherical joints and a ball in cylinder joint and is the solution analyzed in [4-6]. Wang et al. [7] considers the point-line joint obtained using a combination of a spherical joint and a cylinder joint. Dudiţă [8] presents several structural solutions of tripod joints and their structural analysis. Fig. 2, a presents the technical solution upon which Phillips [9] states that can be used as a coupling with approximate constant velocity and affirms that „The mechanics of this joint is complicated. It is not well understood…". The two elements from Fig. 2, a constitute an overconstrained mechanism.

A mechanism with DOF = 1 is presented in Fig. 2, b, where the components are: driven shaft *1*, middle disc with tongue and groove from an Oldham coupling *2*, outer housing (called "tulip") *3*, and the drive shaft (called the "spider") *4*. *B*etween the elements *1*, *2* and *3* there are two prismatic joints acting on normal directions and between the elements *3* and *4* there are three sphere-plane joints. The elements *1* and *4* are connected to the ground via two revolute joints.

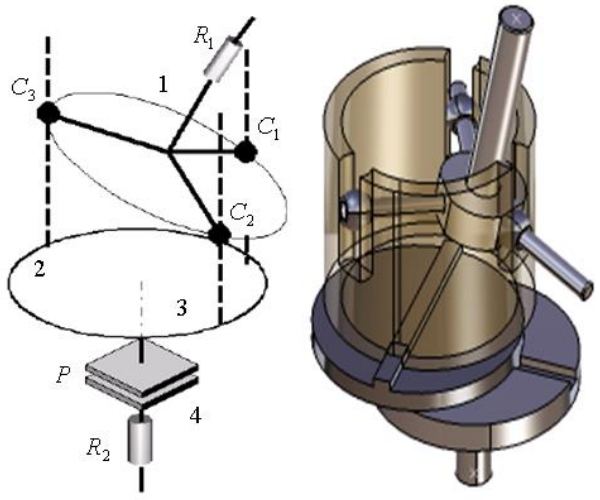

a b

Fig. 1 Homokinetic joint with three point-line joints: a) structural scheme; b) technical solution

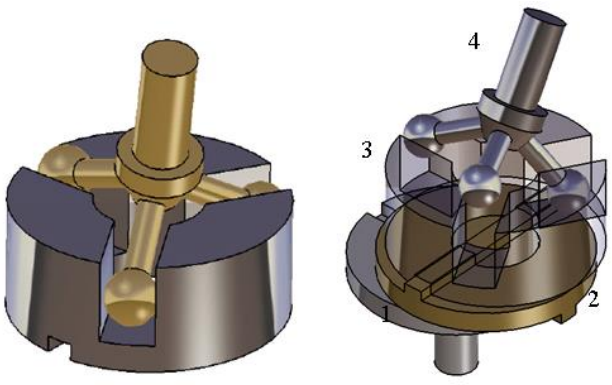

a b

Fig. 2 The 3-ball polycentric tripod joint: a) 3-ball polycentric joint [9]; b) 3-ball polycentric joint used in the actual CV joint

The kinematical analysis of the mechanism obtained using the above polycentric tripod joint is presented subsequently.

3. Kinematical analysis

From Fig. 2, it can be observed that the centers of the spheres will be permanently located in median planes of the grooves in which they are placed. In order to perform a kinematical analysis, the schematization of the mechanisms was made, as seen in Fig. 3. The axes of the two cross shafts are denoted D_1 and D_2. The reference coordinate system is fixed to the ground and has oriented axes. The Oz axis is directed along the straight line D_1 and the Ox axis is the common normal for the straight lines D_1 and D_2. The relative position of the two axes is indicated by the twisting angle α, whose sign is found with respect to the positive sign of Ox axis and the length a of OB, the common normal of the straight lines D_1 and D_2.

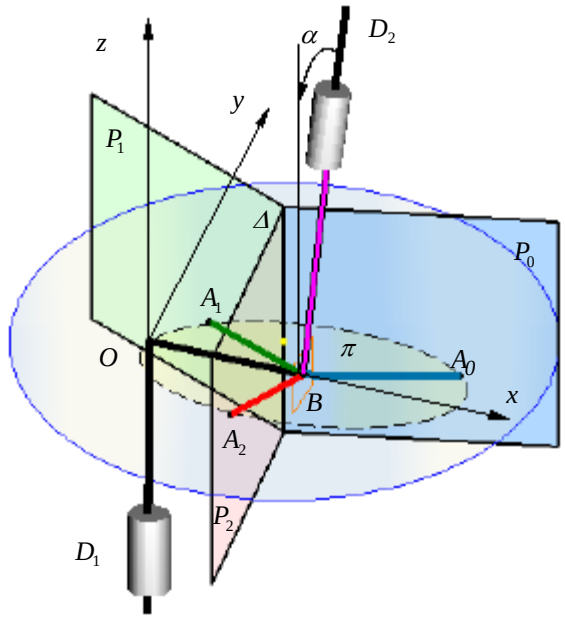

Fig. 3 Scheme for calculus

The elements *1*, *2* and *3* are represented in a simplified manner, by a single element consisting from three planes P_0, P_1, P_2 that have a common side Δ. This element lays on Oxy plane so that the straight line Δ should take any position but constrained to be parallel to Oz axis. The relative position between the three planes is indicated by the interfacial angles γ_1, γ_2, as seen in Fig. 4. The element 4, named "the spider", is represented by three segments BA_k, $k = 0, 1, 2$ having the same length R, positioned in a plane normal to the straight line D_2. The relative position of the segments is given by the angles β_1 and β_2, considered in the plane π.

One considers that the segment OA_0 is revolved in π plane by an angle φ. For completing the mechanism, the point-surface joints between A_k points and P_k planes, $k = 0, 1, 2$ are required. Imposing this condition, the system obtained by planes will take the position given by:

- the coordinates of the intersection point $I(x_0, y_0)$ between the common straight line for the three planes and the plane Oxy;
- the θ angle between the straight line d_0 and Ox axis;
- as a consequence, the angle θ_k formed by the d_k intersection with Oxy plane and the positive half-axis Ox.

$$\theta_0 = \theta, \quad \theta_1 = \theta + \gamma_1, \quad \theta_2 = \theta + \gamma_2 \ . \tag{1}$$

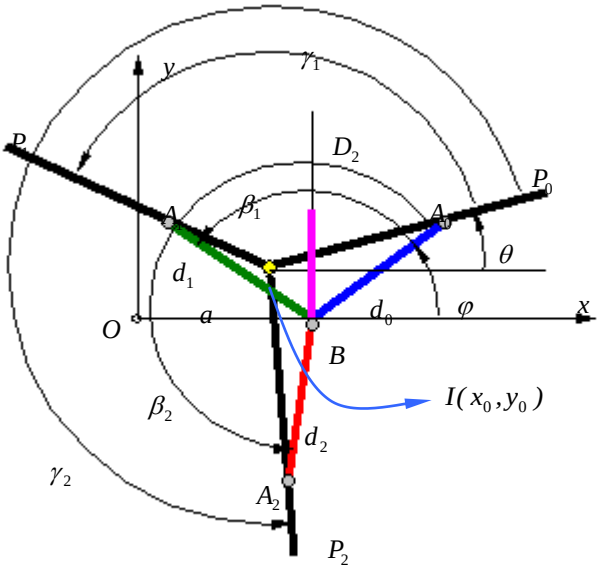

Fig. 4 Kinematical and geometrical parameters of the mechanism

In order to obtain the coordinates of the points $A_k(0,0,R)$ from the systems $Bx'_k y'_k z'_k$, where $Bx'_k \equiv BA_k$, $Bz'_k \equiv D_2$, the homogeneous operators Hartenberg–Denavit are used. According to McCarthy [10] the homogeneous operators corresponding to a screw motion about Ox axis, are:

$$\boldsymbol{X}(\alpha, a) = \begin{bmatrix} 1 & 0 & 0 & a \\ 0 & \cos\alpha & -\sin\alpha & 0 \\ 0 & \sin\alpha & \cos\alpha & 0 \\ 0 & 0 & 0 & 1 \end{bmatrix} \tag{2}$$

and about Oz axis

$$\boldsymbol{Z}(\theta, s) = \begin{bmatrix} \cos\theta & -\sin\theta & 0 & 0 \\ \sin\theta & \cos\theta & 0 & 0 \\ 0 & 0 & 1 & s \\ 0 & 0 & 0 & 1 \end{bmatrix}, \tag{3}$$

respectively, where (α, a) and (θ, s) are the characteristic parameters of the two motions. The coordinates of the points A_k in $Oxyz$ system are:

$$\begin{bmatrix} x_k \\ y_k \\ z_k \\ 1 \end{bmatrix} = \boldsymbol{X}(\alpha, a)\boldsymbol{Z}(\varphi_k, 0) \begin{bmatrix} R \\ 0 \\ 0 \\ 1 \end{bmatrix}, \tag{4}$$

where

$$\varphi_0 = \varphi, \quad \varphi_1 = \varphi + \beta_1, \quad \varphi_2 = \varphi + \beta_2 \ . \tag{5}$$

From relation (5) it is obtained:

$$\begin{cases} x_k = R\cos\varphi_k + a, \\ y_k = R\cos\alpha\sin\varphi_k, \\ z_k = R\sin\alpha\sin\varphi_k. \end{cases} \quad (6)$$

For the plane P_k having the normal unit vector $\boldsymbol{n}_k\left(\cos\delta_k, \sin\delta_k, 0\right)$, the equation is:

$$\boldsymbol{n}_k\left(\boldsymbol{r}-\boldsymbol{r}_0\right)=0, \quad (7)$$

where

$$\delta_k = \theta_k + \pi/2; \quad (8)$$

$$\boldsymbol{r}=[x,y,0],\ \boldsymbol{r}_0=[x_0,y_0,0]. \quad (9)$$

The system (7) is in scalar form, having the unknown θ, x_0, y_0.

$$-\sin(\theta+\gamma_k)(x_k-x_0)+\cos(\theta+\gamma_k)(y_k-y_0)=0. \quad (10)$$

After a series of cumbersome calculus, the solution of the system (10) is, for θ angle:

$$\tan\theta=-\frac{\left[\sin\frac{\beta_2}{2}\cos\left(\varphi+\frac{\beta_2}{2}\right)\Big/\tan\gamma_2-\sin\frac{\beta_1}{2}\cos\left(\varphi+\frac{\beta_1}{2}\right)\Big/\tan\gamma_1\right]\cos\alpha+\sin\frac{\beta_2-\beta_1}{2}\sin\left(\varphi+\frac{\beta_1+\beta_2}{2}\right)}{\sin\frac{\beta_2}{2}\sin\left(\varphi+\frac{\beta_2}{2}\right)\Big/\tan\gamma_2-\sin\frac{\beta_1}{2}\sin\left(\varphi+\frac{\beta_1}{2}\right)\Big/\tan\gamma_1-\sin\frac{\beta_2-\beta_1}{2}\sin\left(\varphi+\frac{\beta_1+\beta_2}{2}\right)\cos\alpha}. \quad (11)$$

Fig. 5 presents the variation of the transmission ratio, $TR=d\theta/d\varphi$, where θ is the position angle of the driven element 3 from Fig. 3, b, known as "tulip" and φ is the input angle φ of driving element 4 from Fig. 3, b, known as "spider". For a particular geometry, Fig. 4, characterized by:

- the angles between the spider's arms, 110°; 100°; 150°;
- spider arms length $R = BA_0 = BA_1 = BA_2 = 50$ mm;
- axes position $\alpha = OB = 30$ mm, ; $\alpha = -30°$;
- the angles between the planes P_k: 100°, 135, 125°, it results $\beta_1 = 100°$, $\beta_2 = 235°$ and $\gamma_1 = 110°$, $\gamma_2 = 210°$ respectively.

From the plot represented in Fig. 5, it is observed that the device doesn't have a constant transmission ratio.

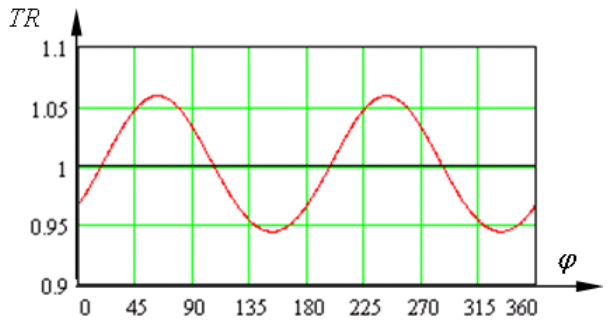

Fig. 5 Variation of transmission ratio (*TR*) versus input rotation angle, φ

The solution for coordinates of $I(x_0, y_0)$ point is:

$$\left.\begin{aligned} x_0 &= \frac{\tan(\theta+\gamma_2)x_2-\tan(\theta+\gamma_1)x_1-(y_2-y_1)}{\tan(\theta+\gamma_2)-\tan(\theta+\gamma_1)}; \\ y_0 &= \frac{(x_2-x_1)+y_1/\tan(\theta+\gamma_1)-y_2/\tan(\theta+\gamma_2)}{1/\tan(\theta+\gamma_1)-1/\tan(\theta+\gamma_2)}. \end{aligned}\right\} \quad (12)$$

From tribological point of view, as it will be shown, is important to know the trajectories of the spheres centers A_k. In the reference system fixed to the element with grooves, the displacement of these points takes place in the symmetry planes. Therefore, in a system with the axis $Oz'' \equiv \Delta$, $Ox''_k \equiv IA_k$, the point A_k has the coordinates $A(x'_k, y'_k, z_k)$ where:

$$\begin{cases} x''_k = IA_k = \left|\boldsymbol{r}_{A_k}-\boldsymbol{r}_I\right| = \sqrt{(x_k-x_0)^2+(y_k-y_0)^2}; \\ y''_k = 0; \\ z''_k = z_k \end{cases} \quad (13)$$

and points A_k in P_k planes, respectively. The correctness of the obtained analytical solutions was verified by comparison with a simulation made via CATIA DMU KINEMATICS module. The trajectory of the point $I(x_0, y_0)$ is represented in Fig. 6, both for analytical solution, relations (12), and for numerical modeling.

The trajectories of the ball centers from the symmetry planes of the grooves are plotted using the relations (13) and there are represented in Fig. 7, a. The numerical solutions are traced in Fig. 7, b-d and in consequence, the numerical model validates the analytical solution.

The CAD model of the joint is presented in Fig. 8 and, on the same figure, there are evidenced the trajectories of the points $I(x_0, y_0)$ and of the centers of the spheres $A_k(x''_k, z''_k)$.

Of special significance is the particular situation when both the grooves and the levers are equidistant, specifically:

$$\gamma_k = k\times 2\pi/3,\ \beta_k = k\times 2\pi/3,\ k=0,1,2. \quad (14)$$

The most important consequence of relations (14) is the fact that, under the given conditions, the mechanism becomes a homokinetic one, thus:

$$\theta=\varphi \quad (15)$$

The transmission ratio is equal to one.

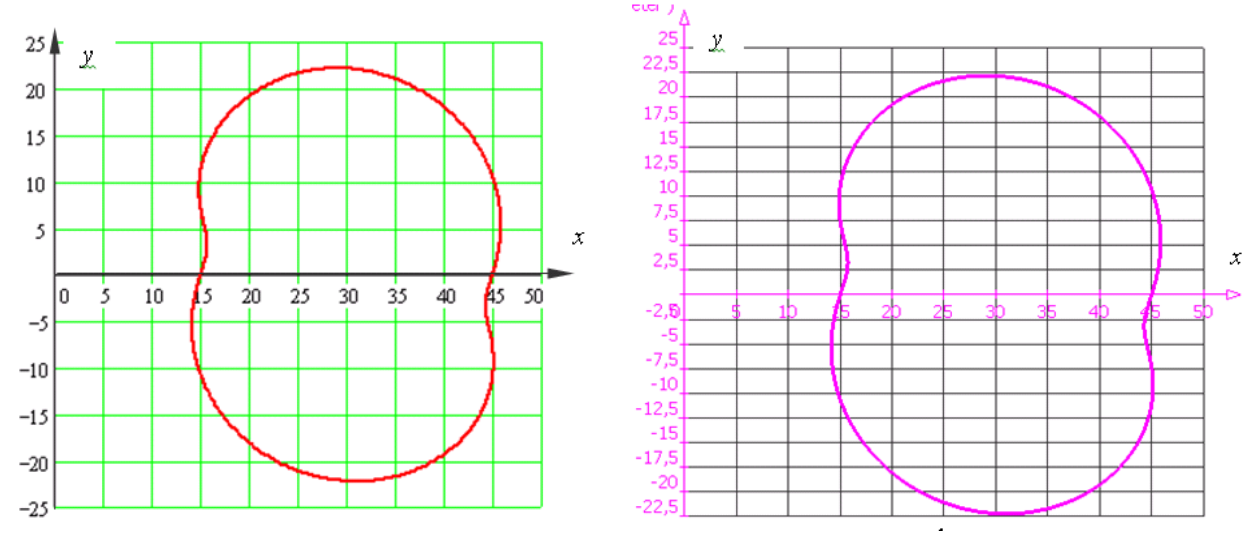

a b

Fig. 6 Trajectory of point $I(x_0, y_0)$ a) analytical results; b) numerical modeling with DMU-Kinematics

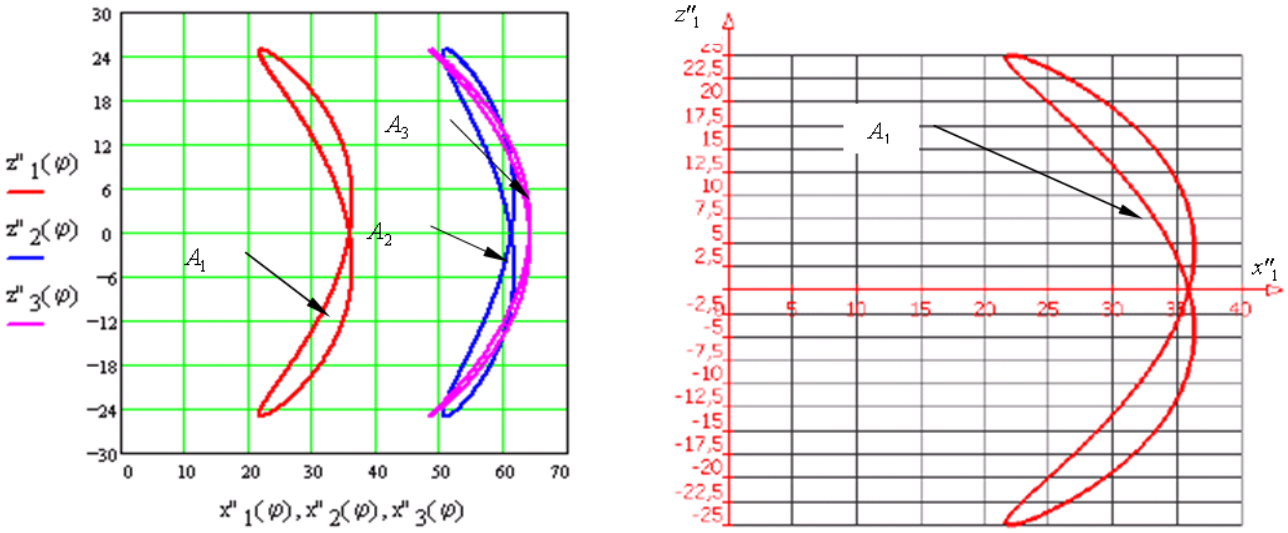

a b

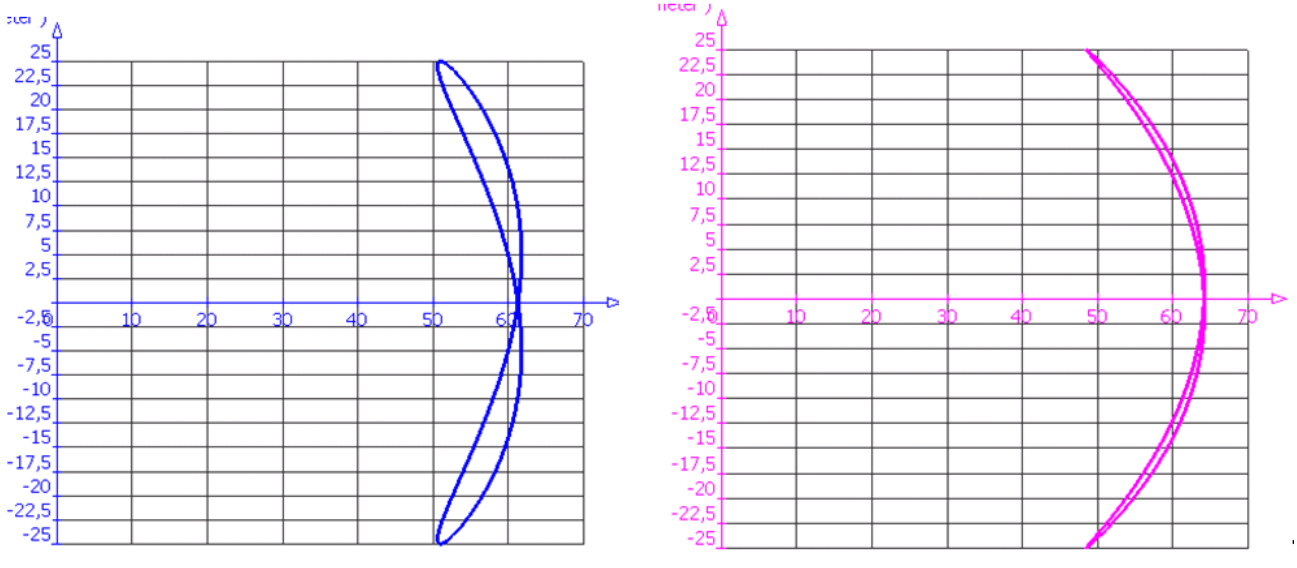

c d

Fig. 7 Trajectories of balls centers $A_k(x''_k, z''_k)$ in the median planes of the grooves: a) analytic solution; b-d) numerical solution

For the particular case described by relations (14), the trajectory of the point $I(x_0, y_0)$ becomes:

$$\begin{cases} x_0 = -\cos 3 \sin^2(\alpha/2) R + a; \\ y_0 = -\sin 3\varphi \sin^2(\alpha/2) R. \end{cases} \quad (16)$$

The relations (16) are the parametric equations of point $I(x_0, y_0)$, that is a circle of radius $R\sin^2(\alpha/2)$ having the center in the fix point $B(a, 0)$.

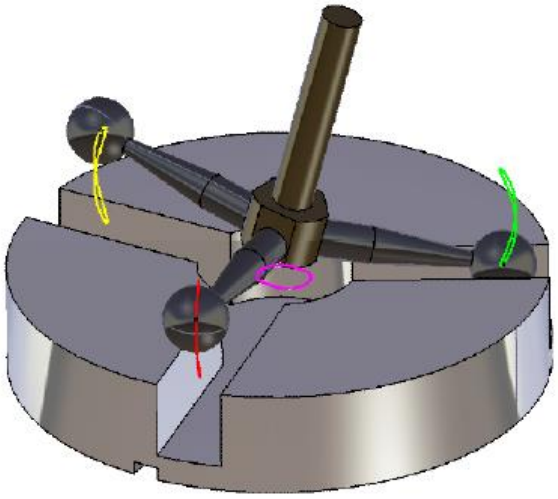

Fig. 8 Trajectories of points I and A_k found by numerical modeling of mechanism's kinematics

The angular velocity of the OI vector is three times the angular velocity of the spider element. In this particular case, the centers of the balls, $A_k(x''_k, z''_k)$, describe identical curves with respect to the tulip element. The parametric equations of these trajectories are:

$$\begin{cases} x''_k = \pm R \sqrt{\cos^4(\alpha/2) + \sin^2\alpha \cos(2\varphi) + \\ +4\sin^4(\alpha/2)\cos^2(2\varphi)}; \\ z''_k = R \sin\alpha \sin\varphi. \end{cases} \quad (17)$$

Under this form, it is difficult to identify the nature of these curves but by eliminating the φ parameter between the above equations, the explicit trajectories equation is obtained:

$$x''_k = \pm\left[\frac{(z/R)^2}{\cos^2(\alpha/2)} - \sin(\alpha/2)^2 - 1\right] R, \quad (18)$$

where from the signs $''\pm''$ must be chosen the one ensuring positive values of x''. As it can be observed from the relation (18), the center of the ball describes parabolic trajectories with horizontal symmetry axis.

4. Proposed structural alternative with lower pairs

Using the mechanism with sphere-plane joints, in its structure is not recommended, as in Fig. 9, a, because the stresses in Hertzian contacts are very high [11]. A first solution proposed for decreasing the contact pressure is presented in Fig. 9, b. In this case, increasing the equivalent contact radius reduces the maximum Hertzian pressure [11] and, as a direct consequence, decreases the von Mises stress. The disadvantage of this solution consist of the fact that, from the five DOF of sphere-plane joint, only the translations are well defined due to the spherical joint between the spider arm sphere and the intermediate element. The middle element has an undeterminate position and may attain a limit situation with unwanted contacts like edge–surface contact.

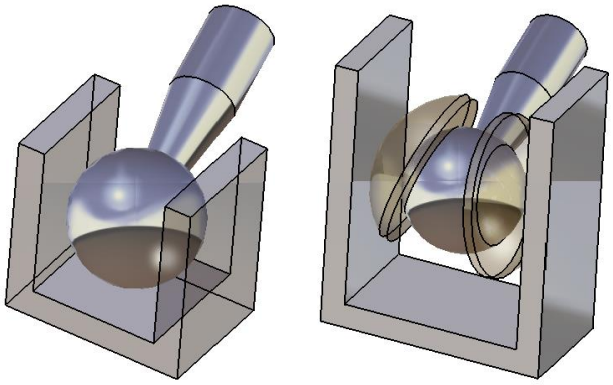

a b

Fig. 9 a) The initial mechanism; b) Solution for reducing the Hertzian contact pressure

With the purpose to eliminate two passive rotations from the sphere-plane contact from Fig. 9, b, a new solution is proposed where there is a contact between two conforming surfaces, the middle element and the groove, Fig. 10, a. The stress state from the proposed solution and the Hertzian case are compared by simultaneous numerical simulation using CATIA Generative Structural Analysis module, Fig. 11. It was considered a package made of a steel ball, radius R = 20 mm, a bronze middle element, with minimum thickness t = 5 mm, pressed by two steel discs of h = 15 mm height.

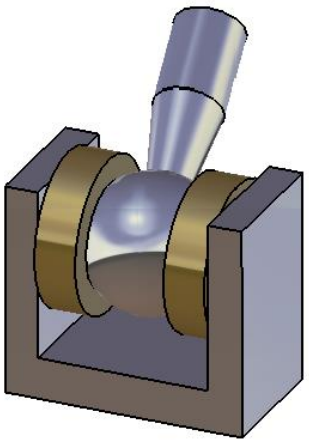

Fig. 10 Solution for contact elements

The normal load was P = 12000 N. A variable mesh finite element analysis was used and a 3 deg assembly wedge [12], as shown in Fig. 11.

The variable meshing ensures that in the contact region the minimum element size is 10^{-4} mm, considerable

smaller than the Hertzian contact radius between the ball and the steel disc, a_{Hz} = 1.16 mm.

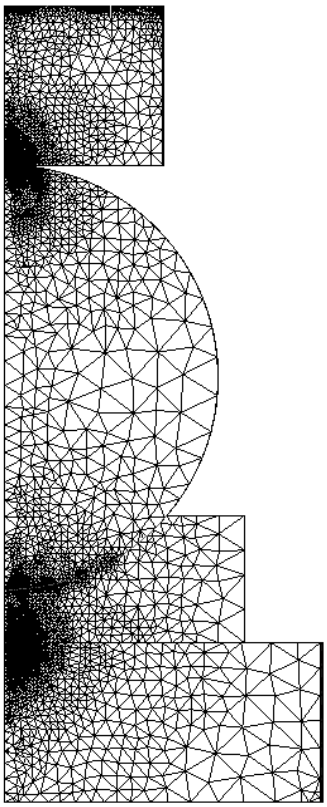

Fig. 11 FEA using variable mesh for the wedge

The stress component on the load direction is presented in Fig. 12 and it can be observed that the maximum stress value, p_{0Hz} = 4.23 GPa occurs in the disc-ball contact and the theoretical value, obtained from analytical relations [11] is p_{0Hza} = 4.26 GPa, and thus, we can consider the numerical model, feasible.

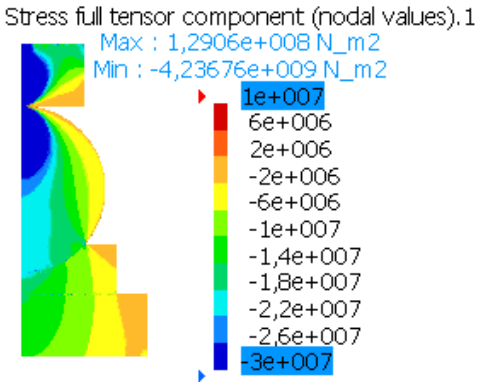

Fig. 12 Normal stresses from FEA

The next step is finding the equivalent von Mises stresses for the final proposed solution, required for wear and failure control [13]. In Fig. 13 there are presented the equivalent von Mises stresses for all components and the maximum is obtained in the point contact. The von Mises stresses for the intermediate element are presented in Fig. 14 and they are at least 100 times lower, compared to the stresses from point contact (Fig. 13).

The middle element acts as a flat-face indenter on the groove's lateral face and due to the edge, there is an effect of increasing normal contact stresses (infinite in theory) in the edge region [11]. This edge effect can be diminished by applying a fillet radius R_f with a value found following the Ciavarella method [13]. The calculus scheme is presented in Fig. 15.

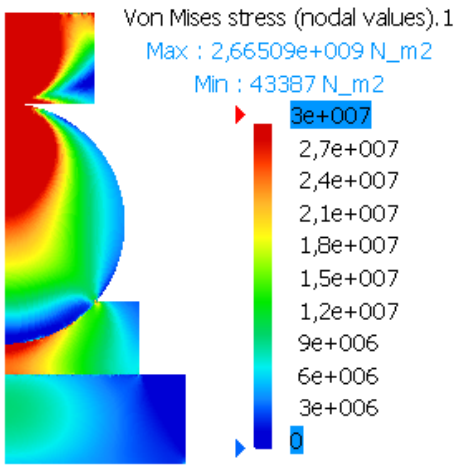

Fig. 13 Von Mises stresses from FEA

Ciavarella, [13], shows that a flat face filleted indenter normally loaded has a higher strength for $b / a < 0.83$, compared to the Hertzian case. For the limit case $b / a = 0.83$ and a fixed load P, the fillet radius can be found by imposing the flat face dimension b equal to the contact radius in the ball-plane Hertzian contact that attains the yield strength limit.

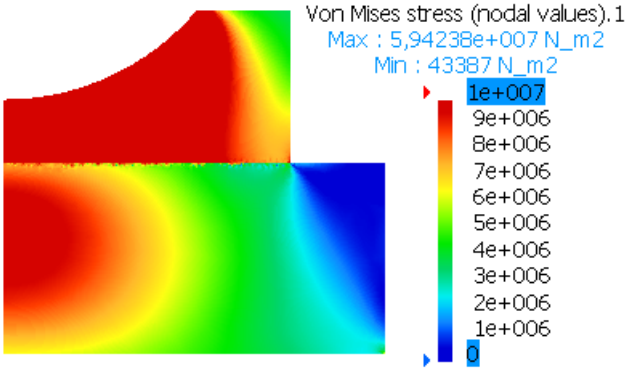

Fig. 14 Von Mises FEA stresses for middle element

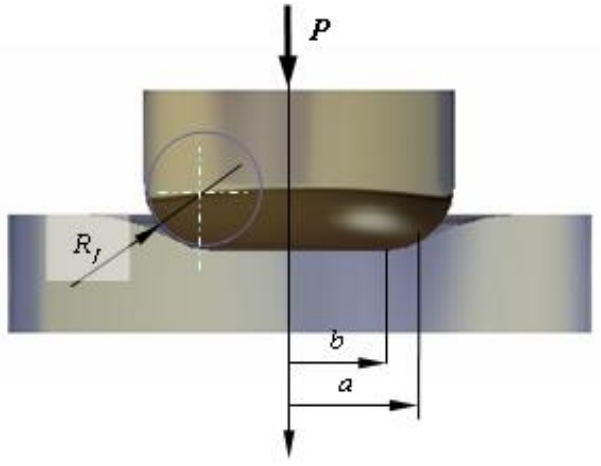

Fig. 15 Flat face filleted indenter [13]

From the strength condition imposed for a Hertzian contact, [13], namely $P/ka_{Hz}^2 = 5.84$, where k is the yield strength in pure shear for normal indentation, for an imposed $b > a_{Hz}$ one can find a and finally, the fillet radius required, R_f, from the following equation:

$$P = \frac{b^3}{3\eta R_f} \frac{3\sin\varphi_0 + \sin^3\varphi_0 - 3\varphi_0 \cos\varphi_0}{\cos^3\varphi_0}, \qquad (19)$$

where

$$\eta = \left(1-\nu_1^2\right)/E_1 + \left(1-\nu_2^2\right)/E_2, \ \cos\varphi_0 = b/a \qquad (20)$$

and $E_{1,2}, \nu_{1,2}$ are the elastic characteristics of the contacting materials.

The constructive solution based on the scheme given in Fig. 15 is presented in Fig. 16. One of the expected advantage of the proposed solution refers to practical aspects, concerning the life time of the assembly - a most important and actual problem.

The middle element, as the most stressed one [14], should be the most wear affected.

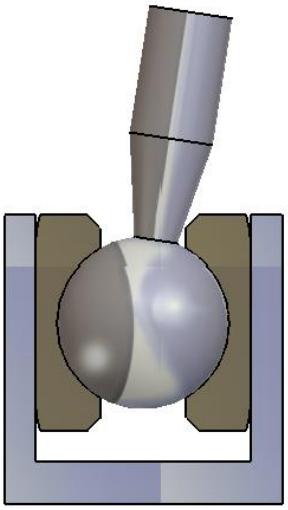

Fig. 16 Final solution with filleted element

At failure, joint reconditioning is a simple replacement of intermediate part.

Moreover, the dimension errors of the groove width can be conveniently corrected by adjusting the dimension of the package made of the spherical end and the two middle elements contacting it.

5. Conclusions

The paper presents a new solution for tripod joint obtained merely via lower pairs. The kinematical analysis is made, for the first time [9] for the general case of the tripod joint. From the advantages of the new solution, it can be mentioned:

- due to the possibility of using only lower pairs in mechanism assembly, the feasibility of the mechanism is a very good one;
- the absence of cylindrical and/or prismatic pairs also reduces the risk of self-locking;
- the input and output shaft axes may take any relative position;
- the input and output shafts are joined to the ground with revolute pairs, this being known as the most practical solution.

The novelty of the paper compared to the existent solutions is given by:

- simple constructive elements bounded by elementary surfaces (plane, cylinder or sphere) technologically feasible and inexpensive, compared, for instance, to "gothic arch" [5];
- a general analytical solution made for mechanism's kinematics applicable was obtained; the relations can be used in the study of constructive errors upon the transmission ration variability;
- the general solutions obtained, applied for the particular case of equidistant arms spider and tulip, prove that the mechanism is a homokinetic one;
- the constructive solution proposed anticipates increased reliability and reduced maintenance costs.

Acknowledgement

This paper was supported by the project "Progress and development through post-doctoral research and innovation in engineering and applied sciences–PRiDE-Contract no. POSDRU/89/1.5/S/57083", project co-funded from European Social Fund through Sectorial Operational Program Human Resources 2007-2013.

References

1. **Sclater, N**. 2011. Mechanisms and Mechanical Devices Sourcebook, 5-th edition, McGraw-Hill Professional; 560 p.
2. **Jacob, W.; Jacob, M.D.** 2006. Rzeppa Joint, United States Patent Application Publication, US 2006/0166751A1. Available from internet: https://docs.google.com/a/google.com/viewer?url=www.google.com/patents/US20060166751.pdf .
3. **Seherr-Thoss, H.; Schmelz, F.; Aucktor E.** 2006. Universal Joints and Driveshafts Analysis, Design, Applications Springer-Verlag Berlin Heidelberg 351 p.
4. **Watanabe, K.; Kawakatsu,T.; Nakao. S.** 2005. Kinematic and Static Analyses of Tripod Constant Velocity Joints of the Spherical End Spider Type, Journal of Mechanical Design 127**:** 1137-1144. http://dx.doi.org/10.1115/1.1909205.
5. **Mariot, J.P.; K'nevez, J.-Y.** 1999. Kinematics of tripode transmissions, A new approach Multibody system dynamics 3**:** 85-105. http://dx.doi.org/10.1023/A:1009852606335.
6. **Urbinati, F.; Pennestrì, E.** 1998. Kinematic and Dynamic Analyses of the Tripode Joint Multibody System Dynamics 2: 355-367. http://dx.doi.org/10.1023/A:1009734924787.
7. **Wang, X.F.; Chang, D.G.; Wang, J.Z.** 2009. Kinematic investigation of tripod sliding universal joints based on coordinate transformation, Multibody System Dynamics,, 22: 97-113. http://dx.doi.org/10.1007/s11044-009-9151-9.
8. **Dudiţă, F.** 1974. Cuplaje mobile homocinetice, (in

Romanian), Ed. Tehnică, Bucuresti, 225 p.
9. **Phillips, J.** 2007. Freedom in Machinery, Cambridge University Press**,** 448 p. http://dx.doi.org/10.1017/CBO9780511751745.
10. **McCarthy. J.M.; Soh G.S.** 2011. Geometric Design of Linkages, Springer, Second Edition, 476 p.
11. **Johnson, K.L.** 1985, Contact Mechanics, Cambridge University Press, 452 p. http://dx.doi.org/10.1017/CBO9781139171731.
12. **Zamani, N.G.** 2008. CATIA V5 FEA Tutorials: Release 17, Schroff Development Corporation, Editor.
13. **Ciavarella, M.** 1999. Indentation by nominally flat or conical indentors with rounded corners, International Journal of Solids and Structures 36: 4149-4181. http://dx.doi.org/10.1016/S0020-7683(98)00186-3.
14. **Bhushan, B.** 2002. Introduction to Tribology, Wiley, 752 p.

S. Alaci, F.C. Ciornei, C. Filote

NAUJA TRIKOJO LANKSTO KONSTRUKCIJA

R e z i u m ė

Straipsnyje pristatoma nauja trikojo (pusašio) lanksto konstrukcija. Kinematinė analizė atlikta analitine forma. Paprastai perdavimo santykis yra kintamas. Sprendinys rastas analitiškai, esant reliatyviems poslinkiams tarp trikojo lanksto elementų, ir leidžia nustatyti reliatyvią rutulinių guolių centrų griovelių simetrijos plokštumose trajektoriją. Analitinius rezultatus patvirtina skaitmeninio modeliavimo rezultatai. Daliniu atveju, esant vienodai nutolusioms trikojo lanksto atramoms ir grioveliams, perdavimo koeficientas tampa pastovus. Transmisiją galima gaminti tik naudojant žemesnes kinematines poras, kas leidžia gerokai sumažinti kontaktinius įtempius, nustatomus baigtinių elementų metodu. Be to, skirtingai negu naudojant esamus mechanizmus su cilindrinėmis jungtimis, sumažėja savaiminio užstrigimo rizika.

S. Alaci, F. C. Ciornei, C. Filote

CONSIDERATIONS UPON A NEW TRIPOD JOINT SOLUTION

S u m m a r y

The paper presents a new solution of tripod joint. The kinematical analysis is obtained for the general case in analytical form. For the general case, the transmission ratio is variable. The solution found for relative displacements between the elements of tripod joint is found analytically and allows obtaining the relative trajectory of the centers of spheres in the symmetry planes of the grooves. The analytical results are validated using an analysis with numerical model. For the particular case of equidistant spider arms and grooves respectively, the transmission ratio becomes constant. The manufacturing of the transmission can be obtained using only lower pairs and thus substantially decreasing the contact stresses, proved by FEA method. Further more, the lack from the actual mechanism of cylindrical joints reduces the risk of self-locking phenomenon.

Keywords: constant transmission ratio, tripod joint, kinematical analysis, finite element analysis.

Received August 21, 2012
Accepted October 10, 2013